Geophysical Research Letters

RESEARCH LETTER
10.1029/2018GL078982

Dipole Types of Autumn Precipitation Variability Over the Subtropical East Asia-Western Pacific Modulated by Shifting ENSO

Chundi Hu[1,2,3], **Dake Chen**[1], **Gang Huang**[2], **and Song Yang**[3,4,5]

[1]State Key Laboratory of Satellite Ocean Environment Dynamics, Second Institute of Oceanography, Hangzhou, China, [2]State Key Laboratory of Numerical Modeling for Atmospheric Sciences and Geophysical Fluid Dynamics, Institute of Atmospheric Physics, Chinese Academy of Sciences, Beijing, China, [3]School of Atmospheric Sciences, Sun Yat-sen University, Guangzhou, China, [4]Guangdong Province Key Laboratory for Climate Change and Natural Disaster Studies, Sun Yat-sen University, Guangzhou, China, [5]Institute of Earth Climate and Environment System, Sun Yat-sen University, Guangzhou, China

Key Points:
- Two different dipole types of autumn precipitation variability are found in the SEAWP during the satellite era
- Changes in the dipole-type precipitation anomaly are linked to shifting ENSO
- Shifting ENSO modulates SEAWP precipitation dipoles mainly via different low-level circulations and the resultant water vapor activities

Supporting Information:
- Supporting Information S1

Correspondence to:
C. Hu,
chundi_nju@yeah.net;
huchd3@mail.sysu.edu.cn

Citation:
Hu, C., Chen, D., Huang, G., & Yang, S. (2018). Dipole types of autumn precipitation variability over the subtropical East Asia-western Pacific modulated by shifting ENSO. *Geophysical Research Letters*, *45*, 9123–9130. https://doi.org/10.1029/2018GL078982

Received 1 JUN 2018
Accepted 27 JUL 2018
Accepted article online 2 AUG 2018
Published online 6 SEP 2018

©2018. The Authors.
This is an open access article under the terms of the Creative Commons Attribution-NonCommercial-NoDerivs License, which permits use and distribution in any medium, provided the original work is properly cited, the use is non-commercial and no modifications or adaptations are made.

Abstract Recent autumns have exhibited two dipole types of precipitation variability (DIPO1 and DIPO2) over the subtropical East Asia-western Pacific (SEAWP). Meanwhile, El Niño–Southern Oscillation (ENSO) has undergone significant mode shift, exhibiting as the eastern Pacific or central Pacific ENSO (EPSO or CPSO). Whether there was any physical linkage between the two remains unclear. Here we demonstrate for the first time that interannual variations of DIPO1 and DIPO2 are closely linked to EPSO and CPSO, respectively. Shifting ENSO modulates the patterns of SEAWP precipitation dipole mainly via changing the path of tropospheric moisture transport and the location of anomalous water vapor convergence/divergence due to different low-level cyclone/anticyclone activities induced by EPSO or CPSO. Further analysis shows that the interdecadal variability of SEAWP precipitation is also linked to the La Niña-like climate shift in 1998. Hence, our study provides some new insight into the ongoing hot debate on the shifting ENSO and increasing autumn drought in southeastern China.

Plain Language Summary We explore the mode changes in the subtropical East Asia-western Pacific (SEAWP) precipitation variability during boreal autumn over 1979–2016, which is important for crop ripening and harvest from the autumn drought perspective. Results show that the eastern Pacific ENSO (El Niño–Southern Oscillation) and central Pacific ENSO primarily drive the DIPO1 and DIPO2 via modifying the low-level atmospheric circulation and moisture response over the SEAWP, respectively. So it should be emphasized that shifting ENSO is responsible for modulating the SEAWP precipitation dipoles to certain extent in the context of global warming.

1. Introduction

As an important season for crop ripening and harvest, autumn precipitation can strongly influence agricultural productions, with remarkable socioeconomic consequences. For example, people in South China witnessed an extraordinarily long-lasting severe drought in autumn 2009, resulting in more than 80 million people suffering direct economic losses of up to 30 billion yuan Renminbi (e.g., Barriopedro et al., 2012; Gu et al., 2015; W. Zhang et al., 2013, 2014). In the context of global warming, more frequent regional autumn droughts occurred over the subtropical East Asia in recent decades (e.g., L. Wang et al., 2015; Wei et al., 2018; W. Zhang et al., 2013, 2014). Meanwhile, more frequent autumn tropical cyclones were observed to generate over the northwestern part of the western North Pacific due to the southwestward shift of the tropical upper-tropospheric trough and the northwestward retreat of the monsoon trough (e.g., Hu et al., 2017; Wu et al., 2015), accompanied by abundant moisture transport and enhanced convective precipitation (Hu et al., 2017). Such cases beg for answers to whether there exists potential resonant interannual variability of precipitation over the subtropical East Asia-western Pacific (SEAWP). In this respect, if there indeed exists resonant interannual variability between subtropical East Asia and western Pacific precipitations, there should be significant synergy anomalies in the same anomaly mode.

On the other hand, it is well known that interannual variations of precipitation and convection over the SEAWP and Maritime Continent are strongly affected by El Niño–Southern Oscillation (ENSO), which link anomalous sea surface temperature (SST) and the resultant low-level cyclone-anticyclone teleconnection

from the Pacific to East Asian in diverse season (e.g., Jia et al., 2016; B. Wang et al., 2000; R. H. Zhang et al., 1996, 1999, 2017; R. H. Zhang & Sumi, 2002; W. Zhang et al., 2011, 2013, 2014). However, the characteristics of ENSO have been changing remarkably, with increasing central Pacific ENSO (hereafter CPSO) under global warming than the traditional eastern Pacific ENSO (hereafter EPSO; e.g., Cai et al., 2015; Capotondi et al., 2015; Lee & McPhaden, 2010; Hu, Yang, Wu, Zhang, et al., 2016; Yu & Kim, 2013) due to natural variability and/or external forcing (Cai et al., 2015; Collins et al., 2010; Yeh et al., 2018), inevitably resulting in changes in ENSO-related atmospheric teleconnections (e.g., Hu, Yang, Wu, Li, et al., 2016; W. Zhang et al., 2011, 2013, 2014; Yeh et al., 2009, 2018). In addition, ENSO activities are strongly modulated by the Pacific Decadal Oscillation (PDO; e.g., Hu et al., 2017; Mantua et al., 1997) and/or the ENSO-like Interdecadal Pacific Oscillation (IPO; e.g., Henley et al., 2015; Power et al., 2006; Y. Zhang et al., 1997). Therefore, we will further examine whether the shifting ENSO and SEAWP precipitation activities have any potential physical linkage.

In the present study, we demonstrate that there are two different dipole types of autumn precipitation anomalies over the SEAWP and that the changes in the dipole types of precipitation anomalies are mainly affected by shifting ENSO via modulating low-level circulations and the resultant anomalous water vapor activities.

2. Data and Methods

Monthly atmospheric data sets are obtained from the ERA-Interim (Dee et al., 2011), with a resolution of 2.5° × 2.5°. The vertically integrated moisture flux (QUV) and the corresponding integrated water vapor transport (IVT) are calculated as follows:

$$\mathrm{QUV} = \frac{1}{g}\int_{200}^{p_s} q\overrightarrow{V}\,\mathrm{d}p;$$

$$\mathrm{IVT} = \sqrt{\left(\frac{1}{g}\int_{200}^{p_s} qu\mathrm{d}p\right)^2 + \left(\frac{1}{g}\int_{200}^{p_s} qv\mathrm{d}p\right)^2}.$$

Here g is the acceleration of Earth's gravity, p_s and p represent the surface pressure and air pressure, respectively, q is the specific humidity, and $\overrightarrow{V}$ indicates horizontal wind vector. Precipitations from the National Oceanic and Atmospheric Administration's Precipitation Reconstruction over Land (Chen et al., 2002) and the Global Precipitation Climatology Project version 2.3 (Adler et al., 2003) over land and ocean are firstly interpolated to grids of 1.25° × 1.25° and then merged together in this study.

Monthly mean SST field is averaged based on the two data sets from the National Oceanic and Atmospheric Administration Extended Reconstructed SST version 5 (2° × 2°; Huang et al., 2017) and the Hadley Centre Global SST (interpolated to 2° × 2°; Rayner et al., 2003), because the averaged SST data favors offsetting the inconsistent signal (or noise) between different data sets to certain extent (Hu, Yang, Wu, Li, et al., 2016). The normalized PDO index is computed from the first principle component (PC) of standardized SST anomalies over the North Pacific (105°E–105°W, 20–60°N) during boreal autumn of 1979–2016, same as in Hu et al. (2017). And the IPO index defined by Henley et al. (2015) is also used (accessed on March 16, 2018 at the website of https://www.esrl.noaa.gov/psd/data/timeseries/IPOTPI). Referring to the Modoki El Niño index defined by Ashok et al. (2007), here an imitative central Pacific ENSO index (CPI) is proposed as follows: CPI = $[\mathrm{SSTA}]_C - 0.5*[\mathrm{SSTA}]_E - 0.5*[\mathrm{SSTA}]_W$, where $[\mathrm{SSTA}]_C$, $[\mathrm{SSTA}]_E$, and $[\mathrm{SSTA}]_W$ represent the area-mean of monthly normalized SST anomalies at each grid over the three regions of (165°E–145°W, 10°S–20°N), (120°–70°W, 10°S–5°N), and (125°–145°E, 0°–25°N), respectively. Following Hu, Yang, Wu, Li, et al. (2016), the eastern Pacific ENSO index (EPI) is defined as the area-mean of monthly normalized SST anomalies at each grid over the region of (140°–80°W, 12°S–5°N).

The empirical orthogonal function (EOF) analysis is employed to capture the first two leading modes of autumn (September–November) precipitation anomalies over the SEAWP (105°–135°E, 12.5°–32.5°N) during 1979–2016. Considering that the local precipitation variances often exhibit significant differentiations in different months and different regions (e.g., the subtropical East Asian versus the subtropical western Pacific precipitations), applying a monthly normalization of the SEAWP precipitation anomaly for each grid prior to the EOF analysis is more suitable and thus to be used in this study. Hence, it should be noted that

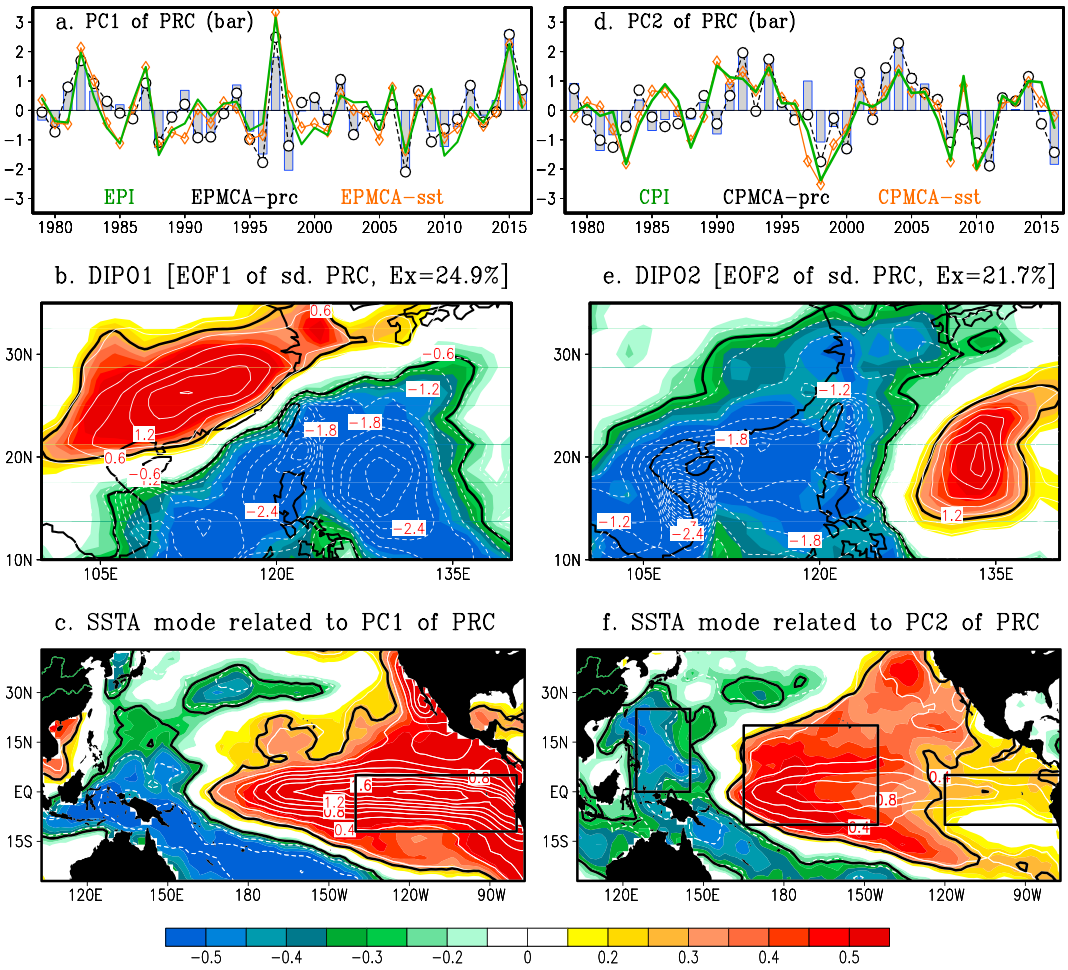

Figure 1. (a) Normalized and detrended PC1, EPI, EPMCA-PRC, and EPMCA-SST. (b) Correlations (shading) and regressions (white curve; 0.5 mm/day) of precipitation associated with PC1 are shown in Figure 1a. (c) Same as Figure 1b except for SST (curve; 0.5 °C). The right panels are the same as the left panels, except for PC2 and for showing the CPI, CPMCA-PRC, and CPMCA-SST in (d). Areas outlined by black thick lines indicate correlation at the estimated 90% confidence level. PC1 = principle component 1; SST = sea surface temperature; EOF = empirical orthogonal function; CPI = central Pacific ENSO index; EPI = eastern Pacific ENSO index; ENSO = El Niño–Southern Oscillation. Black boxes shown in (c) and (f) are the regions used to define the EPI and CPI, respectively (see section 2 for details).

here the EOF decomposition is based on an area-weighted correlation coefficient matrix (rather than a covariance matrix) and that the corresponding eigenvectors are nondimensional. Accordingly, we show the special structures of the two leading EOF modes by regressing and correlating the precipitation anomalies with the corresponding PCs, respectively. Besides, we also use the conditional maximum covariance analysis (MCA; see supporting information Method for details) to confirm the prominence and reliability of the EOF results. The MCA has been widely used for capturing the coupled modes between two physical fields such as atmospheric circulation and SST (e.g., An & Wang, 2005; Ding et al., 2014; Hu, Wu, et al., 2016).

3. Results

3.1. Two Dipole Types of SEAWP Autumn Precipitation

Figure 1 shows the two leading modes of precipitation variability over the SEAWP and the associated SST anomalies. EOF1 and EOF2 (Figures 1b and 1e) exhibit two very different dipole-type patterns of SEAWP autumn precipitation anomalies (named as DIPO1 and DIPO2, respectively), with significant interannual and interdecadal variations (see the PC1 and PC2 shown Figures 1a and 1d, gray bar). The corresponding locally explained variances are specifically shown in Figure S1 (see supporting information Explanation S1 for details). In the current study, a positive phase of DIPO1 is characterized by abundant rainfall over

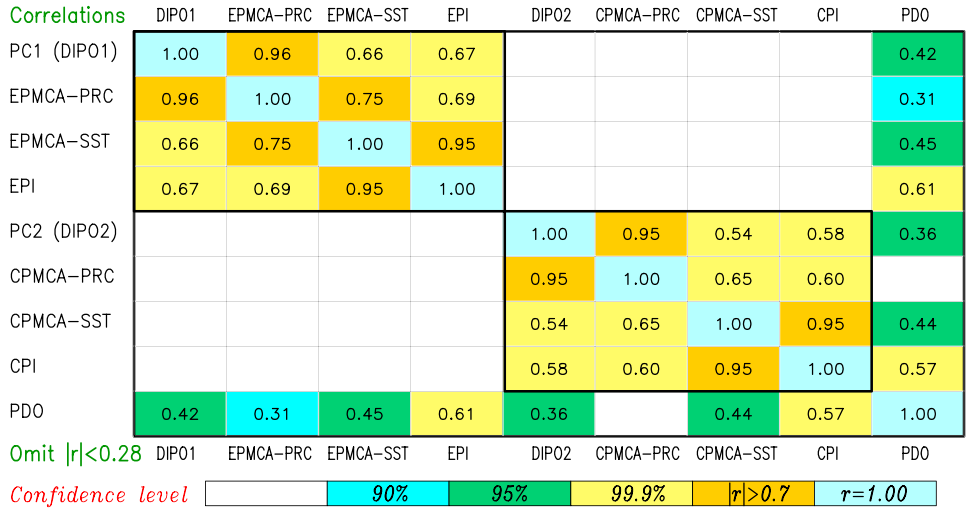

Figure 2. Correlation matrix of DIPO1, DIPO2, MCA-SST/PRC time series, PDO, and two types of ENSO indices. All indices are normalized and detrended. Here only the correlation exceeding the estimated 90% confidence level is shown. ENSO = El Niño–Southern Oscillation; PDO = Pacific Decadal Oscillation; CPI = central Pacific ENSO index; EPI = eastern Pacific ENSO index; SST = sea surface temperature; PC1 = principle component 1.

southeastern China and the northern part of the East China Sea but deficient precipitation over the South China Sea-Philippine Sea (SCS-PS, Figure 1b). In contrast, DIPO2 is featured by prominently weakened rainfall over southeastern Asia, the South China Sea, and the East China Sea but enhanced precipitation to the east of the Philippine Sea (Figure 1e).

Associated with DIPO1 and DIPO2, it is clear that the Pacific SST anomalies are characterized by the classic EPSO and CPSO patterns (Figures 1c and 1f), with maximum SST warming (cooling) over tropical eastern (western) Pacific and central (northwestern) Pacific, respectively. As expected, the associated time series of DIPO1 and DIPO2 (i.e., PC1 and PC2, Figures 1a and 1d) are significantly correlated to EPI and CPI (Figures 1a and 1d, green line) with significant correlations of 0.67 and 0.58, respectively, both exceeding the 99.9% confidence level (Figure 2), suggesting that there are close teleconnections between the types of ENSO and SEAWP rainfall anomaly.

Similar results could be well reproduced by using the conditional MCA, as shown in supporting information Figures S2 and S3. Corresponding to DIPO1 (DIPO2), the time series obtained from the MCA between precipitation and SST (Figures S2 and S3) are referred as EPMCA-PRC and EPMCA-SST (CPMCA-PRC and CPMCA-SST), with a robust correlation of 0.75 (0.65). Furthermore, the correlations between (1) EPMCA-PRC and PC1, (2) EPMCA-SST and EPI, (3) CPMCA-PRC and PC2, and (4) CPMCA-SST and CPI are all high, up to 0.95 (Figure 2), reconfirming that DIPO1 and DIPO2 are indeed closely related to EPSO and CPSO, respectively. It is worth noting that the MCA method is completely independent from the EOF analysis, consequently indicating that the above results about DIPO1 and DIPO2 are prominent and reliable.

3.2. Influence Mechanisms of Shifting ENSO on DIPO1 and DIPO2

To identify the underlying physical mechanism, the changes in the coupled structure of rainfall-ENSO are further analyzed by calculating and contrasting sea level pressure (SLP), 850-hPa wind (UV850), and tropospheric water vapor transport, as shown in Figure 3. During the EPSO/DIPO1 autumn, positive and negative SLP anomalies of the traditional ENSO are quasi-symmetrically distributed on the left and right sides of the International Date Line, respectively (Figures 3a and 3c, shading). Accompanying such distribution of SLP anomalies, there are two adjacent anomalous anticyclones over the Bay of Bengal and the SCS-PS (Figures 3a and 3c, vector), which advect the tropospheric moisture transport into southeastern China and the East China Sea (Figures 3e and 3g, vector). The corresponding water vapor convergence over southeastern China-East China Sea and divergence over the SCS-PS (Figures 3e and 3g, shading) tends to bring more rainfall to southeastern China-East China Sea but less to the SCS-PS, ultimately contributing to the formation of DIPO1 (Figure 1b).

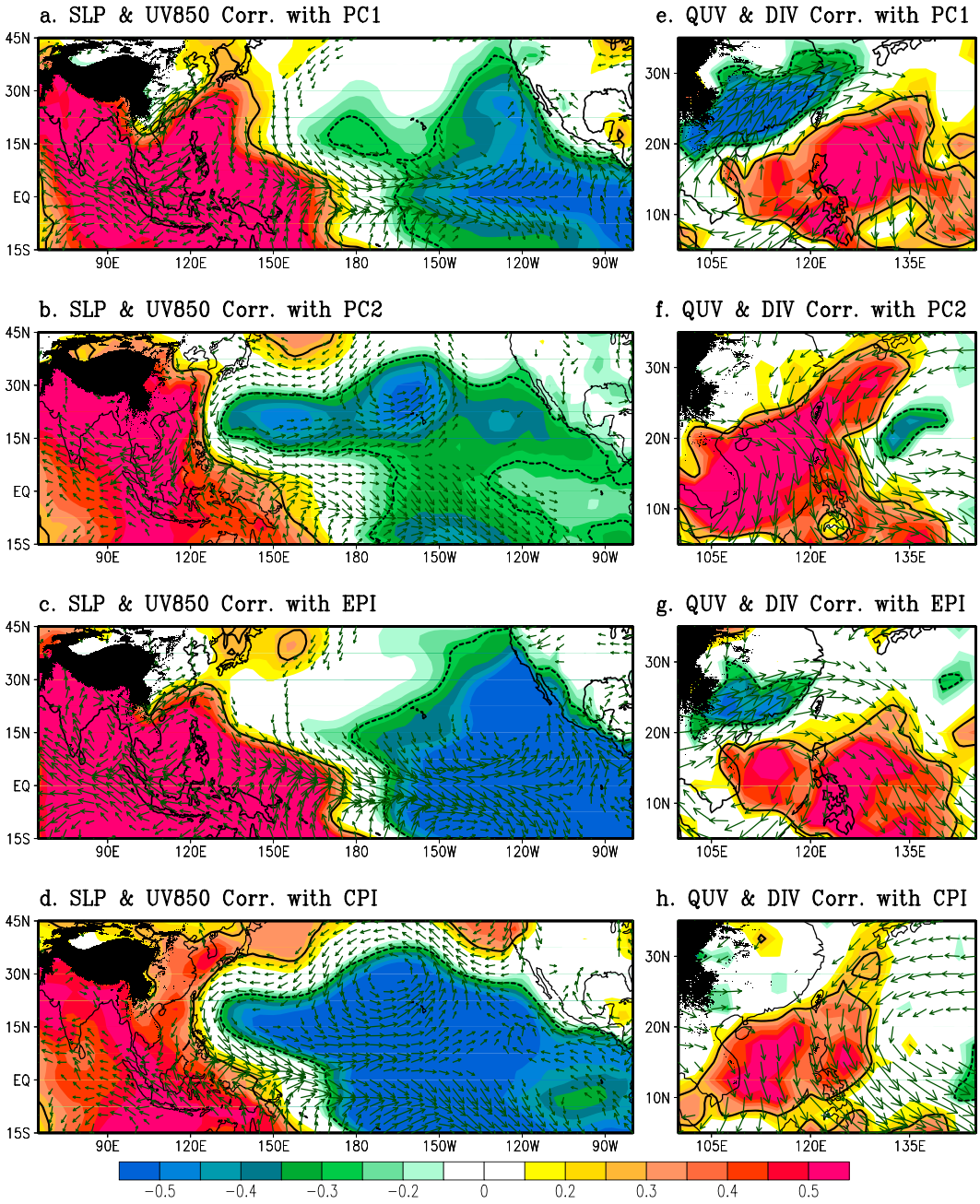

Figure 3. Correlations of UV850 (vector) and SLP (shading) with respect to the normalized and detrended time series of (a) PC1, (b) PC2, (c) EPI, and (d) CPI. The right panels are the same as the left panels, except for showing QUV (vector) and its divergence (shading). Only the vectors with a significant *u* or *v* component over the estimated 90% confidence level are plotted. The thick contour indicates correlation at the estimated 90% confidence level. SLP = sea level pressure; QUV = vertically integrated moisture flux; CPI = central Pacific ENSO index; EPI = eastern Pacific ENSO index; PC1 = principle component 1.

For the CPSO/DIPO2 autumn, the pattern of SLP anomalies related to a malposed ENSO has changed markedly (Figures 3b and 3d versus Figures 3a and 3c, shading), which will inevitably lead to anomalous low-level circulation and moisture transport over the SEAWP: As shown by the vectors in Figures 3b and 3d, the CPSO-related anticyclone over South Asia is weaker and shifts northwestward, relative to the EPSO-related double anticyclone, due to the occurrence of a double subtropical Pacific cyclone (implying a weakened North Pacific Subtropical High). Under the synergy of subtropical anticyclone and cyclone separately located in the west and east of 120°E or so (Figures 3b and 3d), the southerly moisture transport over the SCS-PS is strongly inhibited (Figures 3f and 3h, vector); and the resultant water vapor

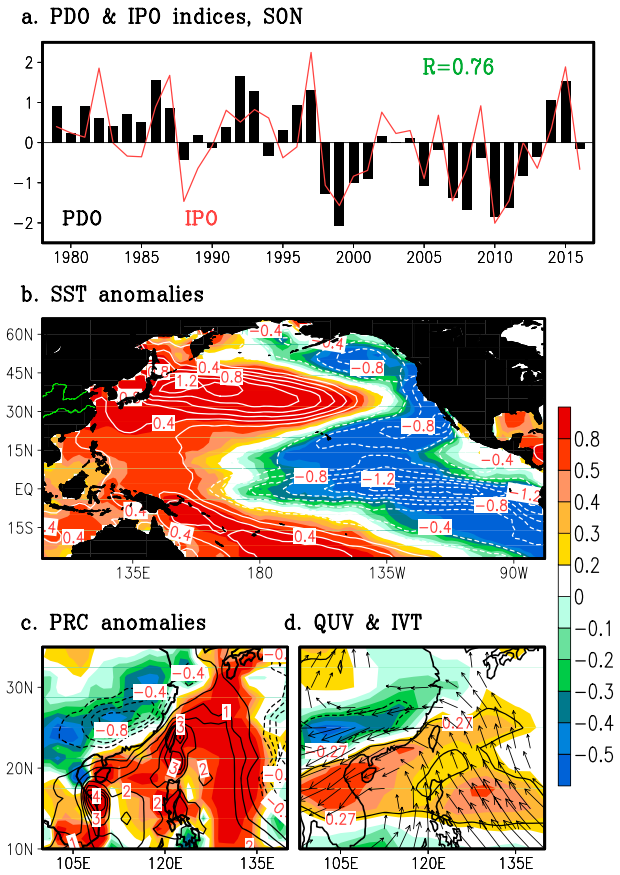

Figure 4. (a) Normalized PDO and IPO indices in autumn. (b) The shadings show decadal changes in SST climatology (1998–2014 minus 1981–1997, 0.5 °C; see supporting information Explanation S3 and Figure S4 for details), and the contours indicate the regression of SST anomalies (0.5 °C) onto the negative PDO index. (c) Interdecadal changes in precipitation (1998–2014 minus 1981–1997; shading, mm/day), and the regression pattern of precipitation anomalies (contour, 0.5 mm/day) onto the negative IPO index. (d) Correlation patterns of QUV (vector) and IVT (shading) with the negative IPO. PDO = Pacific Decadal Oscillation; IPO = Interdecadal Pacific Oscillation; SST = sea surface temperature; IVT = integrated water vapor transport; QUV = vertically integrated moisture flux; SON = September–November.

divergence and convergence (Figures 3f and 3h, shading) greatly favor local precipitation deficit and surplus to generate the DIPO2 (Figure 1e).

4. Discussion and Concluding Remarks

Studies have suggested a significant Pacific climate regime shift since the late 1990s, which has not only led to abrupt interdecadal changes in autumn tropical cyclone activities over the western North Pacific (e.g., Hong et al., 2016; Hsu et al., 2014; Hu et al., 2017; Zhao & Wang, 2016), but also to a change in the relationship between PDO and ENSO since 1998 (e.g., Hu, Yang, Wu, Zhang, et al., 2016; Hu et al., 2017; Jo et al., 2015; Yeh et al., 2018). Here we also find that almost all of the DIPO1- and DIPO2-related precipitation and SST indices shown in Figure 2 are significantly correlated to the PDO, indicating that both the SEAWP precipitation and ENSO activities could be modulated by the 1998 Pacific climate shift (see supporting information Explanation S2).

To confirm such interdecadal change in the SEAWP rainfall-ENSO relationship associated with PDO/IPO, we investigate the relevant interdecadal patterns of autumn SST, SEAWP precipitation, and the corresponding vertically integrated moisture transport (Figures 4a–4d). As expected, both PDO and IPO in autumn (R = 0.76) have undergone a sharp interdecadal change since 1998 (Figure 4a); relevant interdecadal SST anomalies exhibit a La Niña-like mode (Figure 4b) with robust SST warming over the western Pacific-

central North Pacific, which is generally considered to be linked to the late 1990s Pacific interdecadal climate shift (e.g., Hong et al., 2016; Hsu et al., 2014; Hu et al., 2017; Zhao & Wang, 2016). Inspiringly, the corresponding interdecadal patterns of SEAWP precipitation (Figure 4c), integrated moisture flux, and water vapor transport (Figure 4d) also mirror the similar patterns but associated with negative DIPO1 to certain extent (Figures 1b and 3e), further highlighting that the interdecadal variability of SEAWP autumn precipitation is also modulated by the Pacific climate shift in 1998.

By analyzing the oceanic and atmospheric environment changes tied to the SEAWP autumn precipitation variability, we find for the first time that there are two dipole types of SEAWP autumn precipitation anomalies (i.e., DIPO1 and DIPO2), and that their interannual variations are closely linked to EPSO and CPSO, respectively. Concisely, shifting ENSO plays a key role in modulating the Pacific-East Asian teleconnection patterns (via changing the location and intensity of low-level cyclone and anticyclone), which changes the moisture transport path. This is conductive to the different convergence and/or divergence of water vapor in the SEAWP region, favoring different regional precipitation increase and/or decrease, and resulting in different SEAWP precipitation dipoles ultimately. Given the synergy effects of increasingly frequent CPSO under greenhouse warming (e.g., Cai et al., 2015; Hu, Yang, Wu, Zhang, et al., 2016; Lee & McPhaden, 2010; McPhaden et al., 2006; Yeh et al., 2009; Yu & Kim, 2013) and the ENSO-like interdecadal climate shift (e.g., Hong et al., 2016; Hsu et al., 2014; Hu et al., 2017; Y. Zhang et al., 1997; Zhao & Wang, 2016), we project that autumn drought over southeastern China would be more frequent due mainly to the correspondingly changing atmospheric circulations and moisture transport activities (e.g., W. Zhang et al., 2011, 2013, 2014; R. H. Zhang & Sumi, 2002).

Acknowledgments
This research is supported by the National Natural Science Foundation of China (grants 41705050, 41690121, 41690123, 41690120, 41621064, and 41730535); the National Postdoctoral Program for Innovative Talents (grant BX201600039); the China Postdoctoral Science Foundation (grant 2018M630646); the Scientific Research Fund of the Second Institute of Oceanography (grant JB1702); and the National Program on Global Change and Air-Sea Interaction (grant GASI-IPOVAI-04). We appreciate the valuable comments from the anonymous reviewers. We are grateful to all data providers: The ERSST-v5, GPCP-v2.3, and NOAA's PREC/L data products are provided by the NOAA/OAR/ESRL PSD, Boulder, Colorado, USA, available at https://www.esrl.noaa.gov/psd/; the ERA-Interim atmospheric data sets are obtained from http://apps.ecmwf.int/datasets/; and the Hadley SST data is available at https://www.metoffice.gov.uk/hadobs/hadisst/.

References

Adler, R. F., Huffman, G. J., Chang, A., Ferraro, R., Xie, P., Janowiak, J., et al. (2003). The version-2 Global Precipitation Climatology Project (GPCP) monthly precipitation analysis (1979–present). *Journal of Hydrometeorology*, *4*(6), 1147–1167. https://doi.org/10.1175/1525-7541(2003)004<1147:TVGPCP>2.0.CO;2

An, S.-I., & Wang, B. (2005). The forced and intrinsic low-frequency modes in the North Pacific. *Journal of Climate*, *18*(6), 876–885. https://doi.org/10.1175/JCLI-3298.1

Ashok, K., Behera, S. K., Rao, S. A., Weng, H., & Yamagata, T. (2007). El Niño Modoki and its possible teleconnection. *Journal of Geophysical Research*, *112*, C11007. https://doi.org/10.1029/2006JC003798

Barriopedro, D., Gouveia, C. M., Trigo, R. M., & Wang, L. (2012). The 2009/10 drought in China: Possible causes and impacts on vegetation. *Journal of Hydrometeorology*, *13*(4), 1251–1267. https://doi.org/10.1175/JHM-D-11-074.1

Cai, W., Santoso, A., Wang, G., Yeh, S.-W., An, S.-I., Cobb, K. M., et al. (2015). ENSO and greenhouse warming. *Nature Climate Change*, *5*(9), 849–859. https://doi.org/10.1038/nclimate2743

Capotondi, A., Wittenberg, A. T., Newman, M., Lorenzo, E. D., Yu, J.-Y., Braconnot, P., et al. (2015). Understanding ENSO diversity. *Bulletin of the American Meteorological Society*, *96*(6), 921–938. https://doi.org/10.1175/BAMS-D-13-00117.1

Chen, M., Xie, P., Janowiak, J. E., & Arkin, P. A. (2002). Global land precipitation: A 50-yr monthly analysis based on gauge observations. *Journal of Hydrometeorology*, *3*(3), 249–266. https://doi.org/10.1175/1525-7541(2002)003<0249:GLPAYM>2.0.CO;2

Collins, M., An, S.-I., Cai, W., Ganachaud, A., Guilyardi, E., Jin, F.-F., et al. (2010). The impact of global warming on the tropical Pacific Ocean and El Niño. *Nature Geoscience*, *3*(6), 391–397. https://doi.org/10.1038/ngeo868

Dee, D. P., Uppala, S. M., Simmons, A. J., Berrisford, P., Poli, P., Kobayashi, S., et al. (2011). The ERA-Interim reanalysis: Configuration and performance of the data assimilation system. *Quarterly Journal of the Royal Meteorological Society*, *137*(656), 553–597. https://doi.org/10.1002/qj.828

Ding, Q., Wallace, J. M., Battisti, D. S., Steig, E. J., Gallant, A. J. E., Kim, H.-J., & Geng, L. (2014). Tropical forcing of the recent rapid Arctic warming in northeastern Canada and Greenland. *Nature*, *509*(7499), 209–212. https://doi.org/10.1038/nature13260

Gu, W., Wang, L., Li, W., Chen, L., & Sun, C. (2015). Influence of the tropical Pacific east–west thermal contrast on the autumn precipitation in South China. *International Journal of Climatology*, *35*(7), 1543–1555. https://doi.org/10.1002/joc.4075

Henley, B. J., Gergis, J., Karoly, D. J., Power, S. B., Kennedy, J., & Folland, C. K. (2015). A tripole index for the Interdecadal Pacific Oscillation. *Climate Dynamics*, *45*(11–12), 3077–3090. https://doi.org/10.1007/s00382-015-2525-1

Hong, C.-C., Wu, Y. K., & Li, T. (2016). Influence of climate regime shift on the interdecadal change in tropical cyclone activity over the Pacific basin during the middle to late 1990s. *Climate Dynamics*, *47*(7-8), 2587–2600. https://doi.org/10.1007/s00382-016-2986-x

Hsu, P. C., Chu, P. S., Murakami, H., & Zhao, X. (2014). An abrupt decrease in the late-season typhoon activity over the western North Pacific. *Journal of Climate*, *27*(11), 4296–4312. https://doi.org/10.1175/JCLI-D-13-00417.1

Hu, C., Wu, Q., Yang, S., Yao, Y., Chan, D., Li, Z., & Deng, K. (2016). A linkage observed between austral autumn Antarctic oscillation and preceding Southern Ocean SST anomalies. *Journal of Climate*, *29*(6), 2109–2122. https://doi.org/10.1175/JCLI-D-15-0403.1

Hu, C., Yang, S., Wu, Q., Li, Z., Chen, J., Deng, K., et al. (2016). Shifting El Niño inhibits summer Arctic warming and Arctic sea-ice melting over the Canada Basin. *Nature Communications*, *7*, 11721. https://doi.org/10.1038/ncomms11721

Hu, C., Yang, S., Wu, Q., Zhang, T., Zhang, C., Li, Y., et al. (2016). Reinspecting two types of El Niño: A new pair of Niño indices for improving real-time ENSO monitoring. *Climate Dynamics*, *47*(12), 4031–4049. https://doi.org/10.1007/s00382-016-3059-x

Hu, C., Zhang, C., Yang, S., Chen, D., & He, S. (2017). Perspective on the northwestward shift of autumn tropical cyclogenesis locations over the western North Pacific from shifting ENSO. *Climate Dynamics*. https://doi.org/10.1007/s00382-017-4022-1

Huang, B., Thorne, P. W., Banzon, V. F., Boyer, T., Chepurin, G., Lawrimore, J. H., et al. (2017). Extended Reconstructed Sea Surface Temperature version 5 (ERSSTv5), upgrades, validations, and intercomparisons. *Journal of Climate*, *30*(20), 8179–8205. https://doi.org/10.1175/JCLI-D-16-0836.1

Jia, X., Ge, J., & Wang, S. (2016). Diverse impacts of ENSO on wintertime rainfall over the Maritime Continent. *International Journal of Climatology*, *36*(9), 3384–3397. https://doi.org/10.1002/joc.4562

Jo, H.-S., Yeh, S.-W., & Lee, S.-K. (2015). Changes in the relationship in the SST variability between the tropical Pacific and the North Pacific across the 1998/1999 regime shift. *Geophysical Research Letters*, *42*, 7171–7178. https://doi.org/10.1002/2015GL065049

Lee, T., & McPhaden, M. J. (2010). Increasing intensity of El Niño in the central equatorial Pacific. *Geophysical Research Letters*, *37*, L14603. https://doi.org/10.1029/2010GL044007

Mantua, N. J., Hare, S. R., Zhang, Y. Q., Wallace, J. M., & Francis, R. C. (1997). A Pacific interdecadal climate oscillation with impacts on salmon production. *Bulletin of the American Meteorological Society*, *78*(6), 1069–1079. https://doi.org/10.1175/1520-0477(1997)078<1069:APICOW>2.0.CO;2

McPhaden, M. J., Zebiak, S. E., & Glantz, M. H. (2006). ENSO as an integrating concept in Earth science. *Science*, *314*(5806), 1740–1745. https://doi.org/10.1126/science.1132588

Power, S., Haylock, M., Colman, R., & Wang, X. (2006). The predictability of interdecadal changes in ENSO activity and ENSO teleconnections. *Journal of Climate*, *19*(19), 4755–4771. https://doi.org/10.1175/JCLI3868.1

Rayner, N. A., Parker, D. E., Horton, E. B., Folland, C. K., Alexander, L. V., Rowell, D. P., et al. (2003). Global analyses of sea surface temperature, sea ice, and night marine air temperature since the late nineteenth century. *Journal of Geophysical Research*, *108*(D14), 4407. https://doi.org/10.1029/2002JD002670

Wang, B., Wu, R., & Fu, X. (2000). Pacific–East Asian teleconnection: How does ENSO affect East Asian climate? *Journal of Climate*, *13*(9), 1517–1536. https://doi.org/10.1175/1520-0442(2000)013<1517:PEATHD>2.0.CO;2

Wang, L., Chen, W., Zhou, W., & Huang, G. (2015). Teleconnected influence of tropical northwest Pacific sea surface temperature on interannual variability of autumn precipitation in Southwest China. *Climate Dynamics*, *45*(9-10), 2527–2539. https://doi.org/10.1007/s00382-015-2490-8

Wei, T., He, S., Yan, Q., Dong, W., & Wen, X. (2018). Decadal shift in West China autumn precipitation and its association with sea surface temperature. *Journal of Geophysical Research: Atmospheres*, *123*, 835–847. https://doi.org/10.1002/2017JD027092

Wu, L., Wang, C., & Wang, B. (2015). Westward shift of western North Pacific tropical cyclogenesis. *Geophysical Research Letters*, *42*, 1537–1542. https://doi.org/10.1002/2015GL063450

Yeh, S.-W., Cai, W., Min, S.-K., McPhaden, M. J., Dommenget, D., Dewitte, B., et al. (2018). ENSO atmospheric teleconnections and their response to greenhouse gas forcing. *Reviews of Geophysics*, *56*, 185–206. https://doi.org/10.1002/2017RG000568

Yeh, S.-W., Kug, J.-S., Dewitte, B., Kwon, M.-H., Kirtman, B. P., & Jin, F.-F. (2009). El Niño in a changing climate. *Nature*, *461*(7263), 511–514. https://doi.org/10.1038/nature08316

Yu, J.-Y., & Kim, S. T. (2013). Identifying the types of major El Niño events since 1870. *International Journal of Climatology*, *33*(8), 2105–2112. https://doi.org/10.1002/joc.3575

Zhang, R. H., Min, Q. Y., & Su, J. Z. (2017). Impact of El Niño on atmospheric circulations over East Asia and rainfall in China: Role of the anomalous western North Pacific anticyclone. *Science China Earth Sciences*, *60*(6), 1124–1132. https://doi.org/10.1007/s11430-016-9026-x

Zhang, R. H., & Sumi, A. (2002). Moisture circulation over East Asia during El Nino episode in northern winter, spring and autumn. *Journal of the Meteorological Society of Japan*, *80*(2), 213–227. https://doi.org/10.2151/jmsj.80.213

Zhang, R. H., Sumi, A., & Kimoto, M. (1996). Impact of El Niño on the East Asian monsoon: A diagnostic study of the '86/87 and '91/92 events. *Journal of the Meteorological Society of Japan*, *74*(1), 49–62. https://doi.org/10.2151/jmsj1965.74.1_49

Zhang, R. H., Sumi, A., & Kimoto, M. (1999). A diagnostic study of the impact of El Niño on the precipitation in China. *Advances in Atmospheric Sciences*, *16*(2), 229–241. https://doi.org/10.1007/BF02973084

Zhang, W., Jin, F.-F., Li, J., & Ren, H.-L. (2011). Contrasting impacts of two-type El Niño over the western North Pacific during boreal autumn. *Journal of the Meteorological Society of Japan*, *89*(5), 563–569. https://doi.org/10.2151/jmsj.2011-510

Zhang, W., Jin, F.-F., & Turner, A. (2014). Increasing autumn drought over southern China associated with ENSO regime shift. *Geophysical Research Letters*, *41*, 4020–4026. https://doi.org/10.1002/2014GL060130

Zhang, W., Jin, F.-F., Zhao, J. X., Qi, L., & Ren, H.-L. (2013). The possible influence of a non-conventional El Niño on the severe autumn drought of 2009 in southwest China. *Journal of Climate*, *26*(21), 8392–8405. https://doi.org/10.1175/JCLI-D-12-00851.1

Zhang, Y., Wallace, J. M., & Battisti, D. S. (1997). ENSO-like interdecadal variability: 1900–93. *Journal of Climate*, *10*(5), 1004–1020. https://doi.org/10.1175/1520-0442(1997)010<1004:ELIV>2.0.CO;2

Zhao, H., & Wang, C. (2016). Interdecadal modulation on the relationship between ENSO and typhoon activity during the late season in the western North Pacific. *Climate Dynamics*, *47*(1-2), 315–328. https://doi.org/10.1007/s00382-015-2837-1